FRACTURE ENERGIES RELEVANT FOR DRY-SNOW SLAB AVALANCHE RELEASE

Bastian Bergfeld[1]*, Alec van Herwijnen[1], Gregoire Bobilier[1], Jürg Schweizer[1]

[1] *WSL Institute for Snow and Avalanche Research SLF, Davos, Switzerland*

ABSTRACT: In our current understanding of dry-snow slab avalanche release, the crack propagation phase is composed of two parts: first, the onset of crack propagation, i.e. the moment when an initial crack reaches a critical size at which the energy release rate of the system equals the specific fracture energy of the weak layer; second, the dynamic crack propagation phase, when the crack propagates across the slope. To assess the material resistance against crack propagation, one has to know the specific fracture energy. So far, this parameter has only been determined at the onset of crack propagation, and dynamic fracture energy has not yet been measured in snow. This is a relevant property, as during dynamic crack propagation, several processes may modify the fracture energy, and thus potentially stop crack propagation (e.g. crack branching, strain rate effects). With data from long flat field PSTs (up to 9 meters), we suggest a method to assess dynamic fracture energy. Using displacement fields during crack propagation derived from high-speed camera recordings of PSTs, we measured dynamic fracture energies (0.05 to 0.43 J m^{-2}) that were similar to fracture energy measured at the onset of crack propagation (0.1 to 1.5 J m^{-2}). Furthermore, we found that most of the total available energy dissipated during the compaction of the weak layer (30 times more), occurring after initial crack formation. The excess of available energy supplied by the settlement of the slab, was therefore not (viscous-) plastically absorbed in the slab, but in the weak layer itself subsequently to the formation of the primary fracture at the moving crack tip by the compaction of the weak layer. This interpretation of the cracking process is a peculiarity of closing cracks and both energies (dynamic fracture energy and compaction energy) are necessary for sustained crack propagation in flat terrain. Dynamic fracture energy required for the primary fracture that forms the moving crack tip and compaction energy for the subsequent compaction of the weak layer. This work illustrates how complex closing cracks are and that the propensity of the snowpack for self-sustained crack propagation cannot be assessed with typically sized PSTs.

KEYWORDS: Avalanche release, fracture mechanics, weak layer properties, Propagation Saw Test

1. INTRODUCTION

In the last two decades, research on the avalanche release process has made remarkable progress, mainly by recognizing the important role of fracture mechanics while the failure of the weak layer. The introduction of the concept of crack-like collapse phenomena, also known as anticracks, and the development of sophisticated numerical models (e.g., Gaume et al., 2018) and extensive experimental studies (e.g., Bergfeld et al., 2022; van Herwijnen and Jamieson, 2005) have driven this progress. As a result, avalanche formation is no longer seen as a pure shear failure problem (McClung, 1981) but rather as a more complex failure process under mixed-mode loading conditions (e.g. Rosendahl and Weissgraeber, 2020).

The avalanche release process consists of a sequence of failure processes (Schweizer et al., 2003). The first two stages are the initiation and onset of crack propagation. While the initiation process is typically described by the strength of materials concept, the onset of crack propagation is usually described by fracture mechanics models.

No less important for avalanche danger assessment, but much less studied, is the subsequent dynamic crack propagation phase. Dynamic crack propagation is responsible for the fact that a locally triggered relatively small crack within the snowpack propagates in a self-sustained manner so that snow layers on entire slopes can detach and subsequently slide down slope as an avalanche. Dynamic crack propagation thus forms the bridge from the meter to the slope scale (several hundred meters) and determines the size of the avalanche release zone.

However, our understanding of this process is very limited. Comprehensive experimental studies are not available, and the process is mechanically too complex to be well described in analytical models. On the other hand, the process can be studied with numerical models and major advances were recently made (e.g. Trottet et al., 2022). Models based on the material point method and the discrete element method have achieved a computational efficiency such that today's computers are capable of performing three dimensional numerical experiments at the scale required for dynamic crack propagation. Recently pub-

* *Corresponding author address:*
Bastian Bergfeld, WSL Institute of Snow and Avalanche Research SLF, Davos, Switzerland;
tel: +41 81 417 03 54;
email: bastian.bergfeld@slf.ch

lished studies report novel findings and allow new insights (e.g., Bobillier et al., 2021; Trottet et al., 2022). In order to validate these numerical models, field experiments on dynamic fracture propagation are of great relevance and characterizing properties of the snowpack have to be measured in the field.

Therefore, over a 3-month period, we recorded a series of 24 very long PST experiments (up to 9 m long). All tests were performed for the same weak layer and included very different states of the snowpack. High-speed videos of these experiments were analyzed with image correlation techniques to gain insight into the cracking phenomena of a weak layer. Based on these data, we suggest an estimate of dynamic fracture energy, which we call the dissipation of dynamic fracture, by separating the work done in the weak layer ahead of and behind the crack tip.

2. METHODS

2.1 Field experiments

From 4 January to 19 March 2019, we performed 24 propagation saw tests (PST, column width 30 cm) on 22 field days on a flat and uniform site near Davos, Switzerland (Figure 1), located on the roof of a building in a forest opening, protected from wind. The nearby creek, together with the cold concrete roof (snow-concrete interface usually colder than -5 °C) foster the growth of surface hoar. In addition, direct sunlight does not reach the field site until end of February. These factors make the site an ideal outdoor laboratory for crack propagation experiments under relatively controlled snowpack conditions. In all PSTs, we tested the same weak layer, consisting of surface hoar (10-15 mm, crystal size and weak layer thickness) that had formed during multiple days at the end of December 2018. This layer of surface hoar was buried by consecutive snowfalls at the beginning of January 2019. Slab thickness increased over the measurement period. On every field day, we characterized the snowpack with a manual snow profile following Fierz et al. (2009). To measure snow density, we used a 100 cm^3 cylindrical density cutter (38 mm diameter). To assess snowpack variations along the PSTs, we performed snow micro-penetrometer measurements approximately every 50 cm. Generally, variations in penetration resistance along the PST column were small.

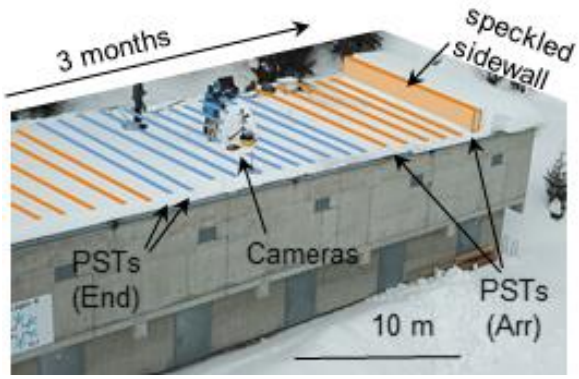

Figure 1: Field site where we performed numerous propagation saw tests (PSTs) resulting either in full propagation (“End”, blue) or crack arrest (“Arr”, orange). Each PST was filmed with a high-speed camera.

One sidewall of each PST experiment was recorded with a high-speed camera (Phantom, VEO710, 1280 pixel horizontal resolution). The side wall of the PST was speckled with black ink (Indian Ink, Lefranc & Bourgeois) to enhance the contrast for digital image correlation (DIC) analysis. The camera was aligned perpendicular to the centre-point of the PST wall. Camera distortion correction, DIC analysis and preprocessing (pixel to meter conversion, identifying slab, weak layer and substratum) were done as described in Bergfeld et al. (2021). Camera settings and settings for the DIC analysis can be found in Bergfeld et al. (2023).

The DIC analysis of the recorded high-speed videos provided us with the vertical (w) and horizontal (u) displacement fields of the PST sidewall with time. Time resolution is given by the frame rate of the recordings (3000 – 22 000 for the high-speed camera, (see Table 4.A1 in Bergfeld et al., 2023). Spatial measurement resolution (6-27 mm) is given by the step-size of the subsets used for DIC analysis (see Table 4.A2 in Bergfeld et al., 2023) and the pixel-to-meter conversion factor (see Table 4.A1 in Bergfeld et al., 2023). In a further pre-processing step, we calculated time derivatives from high-speed displacement fields to obtain velocity ($\dot{w}$, $\dot{u}$) and acceleration $\ddot{w}$ and $\ddot{u}$ of the slab.

2.2 Dissipation of dynamic fracture and compaction

The process of a propagating closing crack (also called anticrack) can be seen as illustrated in Figure 2. Ahead of the crack tip, in undisturbed parts of the slab (region I in Figure 2) a beam section (exemplified in Figure 2) is fully supported by the weak layer. The slab-weak layer system is in a static configuration (Figure 2 and Figure 3a, region I). From a microstructural perspective, the weak layer support

comes from “load chains”, e.g. single ice structures carrying small portions of the overall static load of the beam section. As the crack tip approaches, load chains in the weak layer, below a beam section, consecutively fail. The beam section starts to move downward (Figure 2 and Figure 3a, region II). Subsequently, the advancing downward movement further breaks weak layer bonds, but with closer packing it also builds up an increasing number of new bonds in the weak layer (Figure 2 and Figure 3a, region III). Hence, during this compaction phase the supporting force of the weak layer increases and brings the beam section back to rest (Figure 2 and Figure 3a, region IV).

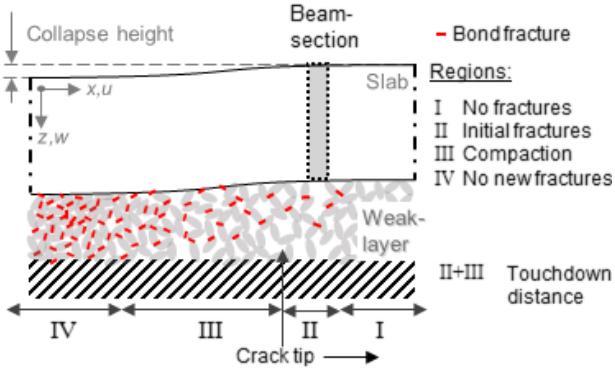

Figure 2: Schematic representation of a running crack in our flat field PST experiments. The crack tip propagates from left to right. In region I, weak layer bonds are not yet fractured, while in region IV all weak layer bonds are broken (red lines). Region II is the fracture process zone, extending from the first bond fractures to the crack tip. In region III, the slab further subsides causing the weak layer structure to fracture multiple times before closer packing of the weak layer is achieved and the slab comes to rest again.

Comparing this schematic process of a closing crack with an opening crack (e.g. normal mode I crack), the energy needed to fracture the weak layer in region II seems to be analogous to the specific dynamic fracture energy of opening cracks. For opening cracks, energy dissipation in the weak layer originates only from crack growth and associated physical processes such as surface creation and localized plastic deformation. A closing crack, however, dissipates additional energy behind the crack tip due to secondary fractures and friction during the compaction phase (region III). That is, there are two sources of energy dissipation. The latter we call the dissipation of compaction. The energy required to form the crack in the fracture process zone (region II) as the dissipation of dynamic fracture.

Assuming that the slab and substratum are in the same stress state before and after crack propagation, slab and substratum contain the same amount of strain energy. This assumption cannot easily be verified, but within the limits of our measurement uncertainty, we did not observe residual strain in the slab and substratum. Hence, it is reasonable to assume that the total energy dissipated in the weak layer (dissipation of dynamic fracture and compaction) equals the released gravitational potential energy of the slab plus the elastic potential energy of the weak layer.

To separate the dissipation of dynamic fracture from the compaction part, we considered small beam sections within the slab of the PST (Figure 2, grey area in slab). Every beam section is regarded as behaving like a free body, not attached in the structural compound.

As the crack tip separates the fracture process zone and the compaction zone, an estimate of the location of the crack tip is required. Therefore, we follow the schematic process of crack propagation and define the crack tip as the point where all initial load chains failed and there is virtually no support yet of new contacts, it is the point where the downward acceleration of the beam section is highest. It was confirmed by numerical simulations that this crack tip definition is equivalent to other definitions of crack tip (see Appendix C in Bergfeld et al., 2023).

We define the time t_0 when the peak in the acceleration is reached as the time the crack tip is at the beam section (Figure 3a, black dot). Everything before t_0 is attributed to the initial fracture (dissipation of dynamic fracture), while everything after t_0 is part of the compaction phase (dissipation of compaction).

Considering the displacement of the beam section, initially it is at rest with zero displacement (Figure 3a, $t \leq 205$ ms). The supporting force F_s is then equal to the gravitational force F_g, induced by the weight of the beam section. Shortly before the crack tip reaches the beam section (Figure 3b, region II), the supporting force F_s decreases and equals the difference between the gravitational force and the acceleration force F_a of the beam section:

$$F_s = F_g - F_a = m\,(g - \ddot{w}), \qquad (1)$$

where m is the mass of the beam section. For $t > t_0$, in region III, the weak layer is compacted and slab support increases. When $F_a/F_g > 1$ (Figure 3b), the slab decelerates before coming to rest again for $t > 310$ ms (Figure 3a).

In each time step Δt, the beam section displaces by Δw. This means that during Δt the work ΔE^{wl} done to destroy the weak layer along Δw can be computed as:

$$\frac{\Delta W^{wl}}{\Delta t} = F_s \frac{\Delta w}{\Delta t}, \qquad (2)$$

$$W^{\mathrm{wl}}(t) = \sum_{t} \Delta W^{\mathrm{wl}}, \qquad (3)$$

Summing up the increments ΔW^{wl} provides the total work $W^{\mathrm{wl}}(t)$ a beam section did to fracture and compact the weak layer (Figure 3d).

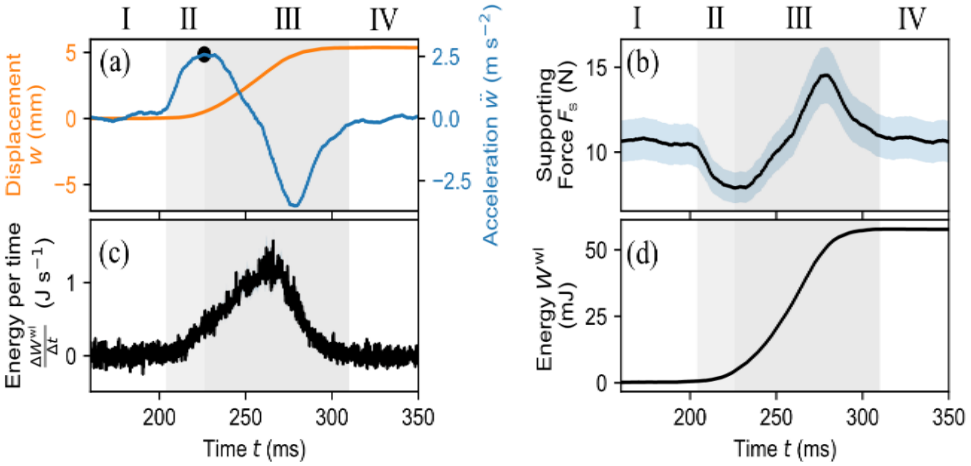

Figure 3: (a) Vertical displacement *w* (orange) and acceleration (blue) with time for a beam section in a PST experiment. (b) Supporting force $\boldsymbol{F_s}$ with time. (c) The power $\frac{\Delta \boldsymbol{W^{wl}}}{\Delta \boldsymbol{t}}$ which destroys the weak layer as the beam section displaces. (d) The total work $\boldsymbol{W^{wl}(t)}$ done to fracture (region II) and compact (region III) the weak layer. The grey shaded backgrounds separate the regions I to IV defined in Figure 2.

Separating the work done in region II and III, provides the work done to initially fracture the weak layer in the fracture process zone $W^{\mathrm{frac}}(x)$ from the work done to subsequently compact the weak layer $W^{\mathrm{comp}}(x)$. Both depend on the *x*-location of the beam section and on the width *b* and length *l* of the beam section, where $A = b\,l$ is the area of the beam section which is in contact with the weak layer. Therefore, we define a specific dissipation of dynamic fracture $w_{\mathrm{f}}^{\mathrm{dyn}} = {W^{\mathrm{frac}}(x)}/{A}$, and a specific dissipation of compaction as $w_{\mathrm{comp}} = {W^{\mathrm{comp}}(x)}/{A}$ (Figure 4).

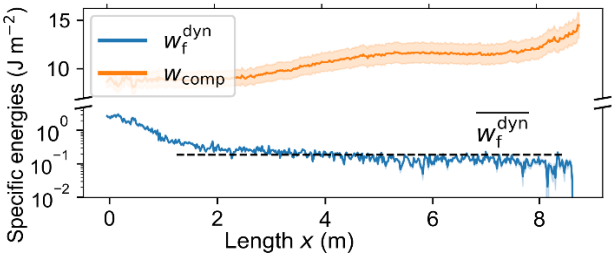

Figure 4: Specific dissipation of dynamic fracture (blue) and specific dissipation of compaction (orange) over the entire crack propagation length in a PST experiment.

To neglect edge effects from both ends of the PST column, we manually picked a distance along the column where the specific dissipation of dynamic fracture was almost constant (Figure 4, black dashed line) and computed the mean specific dissipation of dynamic fracture $\overline{w_{\mathrm{f}}^{\mathrm{dyn}}}$ for this distance. Uncertainties in displacement and acceleration of beam sections prior to crack propagation were estimated as the standard deviation. The uncertainties were propagated through Equations 1 to 3 using Gaussian error propagation.

3. RESULTS AND DISCUSSION

On average, the specific dissipation of compaction was 30 times higher than the specific dissipation of dynamic fracture, indicating that the majority of the energy is used for weak layer crushing and not for advancing the crack in the weak layer (Figure 5a and b, respectively). The specific dissipation of dynamic fracture generally increased with time. On 7 January it was $5 \pm 16 \times 10^{-3}$ J m^{-2} and at the end of the measurement series on 19 March it was 0.43 ± 0.19 J m^{-2} (Figure 5a). These values are in the same range as the static weak layer specific fracture energy w_f derived from the same experiments (Figure 8a in Bergfeld et al., 2023).

The dissipation of dynamic fracture had two local maxima with time (Figure 5a), first around 15 January, and second around 18 February. The dissipation of dynamic fracture is not necessarily a material property of the weak layer, as it may also depend on crack propagation characteristics, such as crack speed. The high values of fracture energy around 15 January were well correlated with higher crack

speeds (compare Bergfeld et al., 2023, Figure 10a), hence higher propagation speeds may lead to higher dissipation of dynamic fracture as it was also observed in bones (Behiri and Bonfield, 1980) or some engineering plastics (e.g., Fond and Schirrer, 2001)). On the other hand, the second maximum on 18 March was not characterized by a high crack speed and this experiment resulted in crack arrest. We therefore attribute the observed fluctuations in the dissipation of dynamic fracture to the method we used to separate dissipation of dynamic fracture from the compaction part. Analogous to opening cracks, we envisioned and estimated dissipation of dynamic fracture as the energy dissipated in the weak layer ahead of the crack tip (uncracked region). For opening cracks, this is close to the total energy dissipated in the weak layer, since there is typically no energy dissipation in the weak layer behind the crack tip (cracked region). In the case of closing cracks, more energy is dissipated in the weak layer behind the crack tip to crush the weak layer, what we call dissipation of compaction. This is not only a material property of the weak layer, but a quantity that likely depends on the entire system of slab, substratum, weak layer and slope angle. Our estimates for the dissipation of dynamic fracture are therefore closely related to our definition of the crack tip and the associated amount of settlement (amount of interpenetration) at the crack tip.

This settlement comes along with a reduction in the volume of the weak layer, a volumetric fracture energy might, therefore, be more appropriate than the classical energy per area. As alternative to the specific dissipation of dynamic fracture, expressed as an energy per fractured area, we therefore computed a volumetric fracture dissipation expressed as the energy needed to compact the weak layer (Figure 5c). To do so, we divided the specific dissipation of dynamic fracture by the settlement of the slab at the crack tip (see Figure 3a):

$$\overline{w_{\mathrm{f}}^{\mathrm{vol.\ dyn}}} = \overline{w_{\mathrm{f}}^{\mathrm{dyn}}} \Big/ w(t(\max(\ddot{w})) \quad (1)$$

This volumetric dissipation of dynamic fracture is the energy per destroyed/compacted volume, a measure that seems more intuitive for closing cracks. Overall, the volumetric dissipation of dynamic fracture increased with time from 1 ± 4 kJ m^{-3} to 2.7 ± 0.6 kJ m^{-3}. For the volumetric dissipation of dynamic fracture, the earlier mentioned maxima in January and March disappeared, and there were overall less fluctuations with time (Figure 5c).

However, the computed volumetric dissipation of dynamic fracture only accounts for mode I contributions, as we only considered the vertical displacement. In our flat field experiments, this is probably not problematic. Bobillier et al. (2021) showed that during dynamic crack propagation in the flat, the shear stress at the crack tip are small compared to the compressive stress. We thus expect that the contributions of Mode II energy dissipations should also be small in the flat. For PST experiments on slopes, the applied methodology will therefore have to be adapted to incorporate the mode II contributions in the volumetric dissipation of dynamic fracture.

Specific dissipation of dynamic fracture (and the volumetric one) did not depend on the outcome of the PST as values from full propagation and crack arrest aligned well in the temporal trend. The specific dissipation of compaction, on the other hand, was significantly lower for PSTs resulting in crack arrest than for PSTs resulting in full propagation (Figure 5b), on average 2 ± 0.3 J m^{-2} and 10.1 ± 0.4 J m^{-2}, respectively. (Figure 5b, orange and blue dots, respectively). In PSTs with crack arrest no stable crack propagation occurred, even if the crack propagated several meters. The collapse height decreased steadily towards the crack arrest point. Therefore, it is not surprising that the dissipation of compaction in PSTs resulting in crack arrest was also lower as the overall settlement was much lower (Figure 5b). This suggests that the dissipation of compaction as defined in our method is not a material property of the weak layer, but rather a property of the entire system.

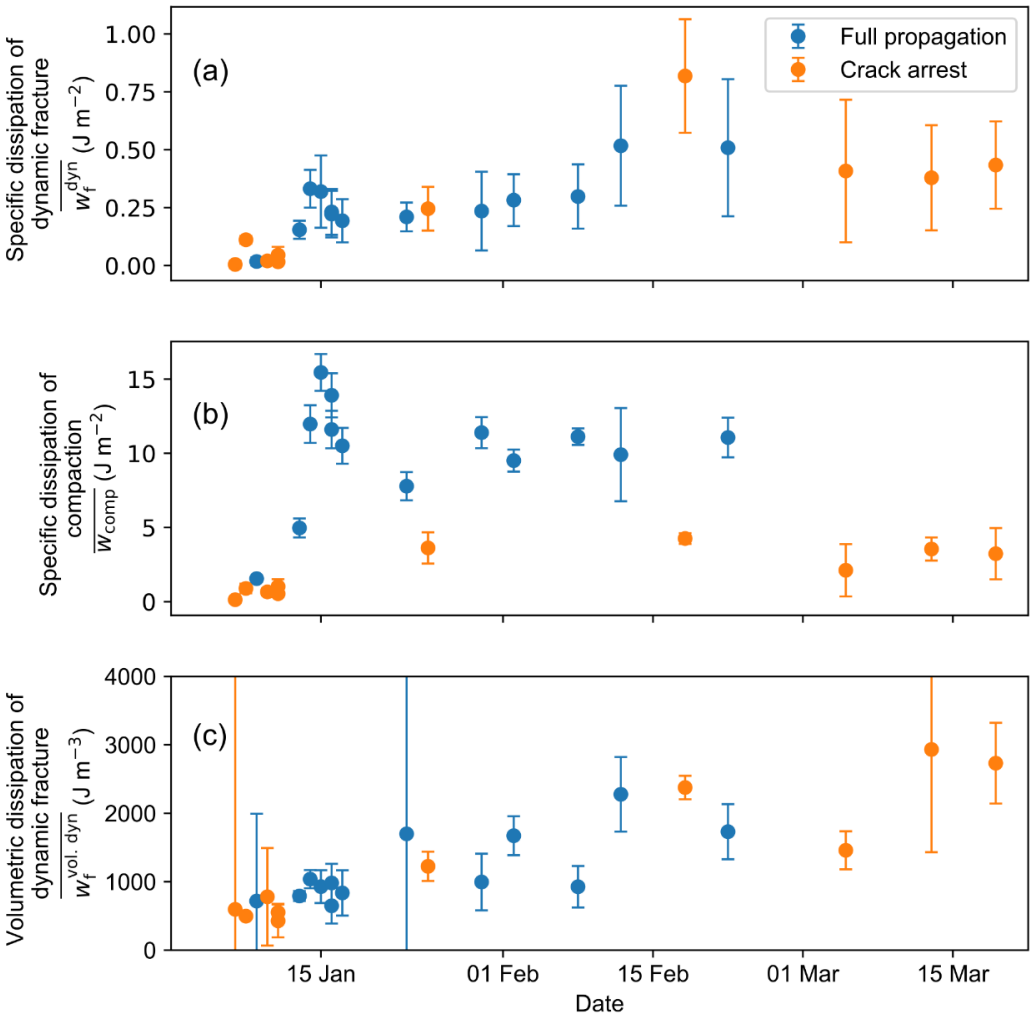

Figure 5: a) Specific dissipation of dynamic fracture ($\overline{w_f^{dyn}}$) with time. (b) Specific dissipation of compaction ($\overline{w_{comp}}$) with time. (c) Volumetric dissipation of dynamic fracture ($\overline{w_f^{vol.\ dyn}}$) with time. PST results are shown with different colors: full propagation (blue dots) or crack arrest (orange dots). Error bars indicate the measurement uncertainty.

4. CONCLUSION AND OUTLOOK

The specific fracture energy estimated from the onset of crack propagation (static fracture energy) does not necessarily coincide with the required energy during dynamic propagation (Freund, 1990). As the dissipation of dynamic fracture in closing cracks is superimposed with the dissipation of compaction, we suggested to separate the work done in the weak layer into a dissipation of dynamic fracture and the dissipation of compaction. The dissipation of dynamic fracture is absorbed in the fracture process zone ahead of the crack tip, and the dissipation of compaction is absorbed after the crack tip passed, and the slab further bends down and settles.

Dissipation of compaction was 30 times higher than the dissipation of dynamic fracture (5 × 10^{-3} J m^{-2} to 0.4 J m^{-2}) which was in the same range as the static specific fracture energy of the weak layer. As the dissipation of dynamic fracture and compaction is inherently linked to a certain amount of interpenetration of the weak layer, we alternatively computed a volumetric dissipation of dynamic fracture. The volumetric dissipation of dynamic fracture (1 to 2.7 kJ m^{-3}) exhibited a steadier increase during the measurement series and was therefore deemed to be a useful quantity to express the resistivity of the weak layer against closing cracks.

Overall, the presented data allowed us to better understand the energy dissipation processes during anticrack growth and are valuable for validation of numerical models.

5. ACKNOWLEDGEMENT

Achille Capelli, Christine Seupel, Colin Lüond, Alexander Hebbe, Simon Caminada, Bettina Richter and Stephanie Mayer assisted with fieldwork. This research has been supported by the Swiss National Science Foundation (grant no. 200021_169424)

REFERENCES

Behiri, J.C. and Bonfield, W., 1980. Crack velocity dependence of longitudinal fracture in bone. J. Mater. Sci., 15: 1841–1849.

Bergfeld, B., van Herwijnen, A., Bobillier, G., Larose, E., Moreau, L., Trottet, B., Gaume, J., Cathomen, J., Dual, J. and Schweizer, J., 2022. Crack propagation speeds in weak snowpack layers. J. Glaciol., 68(269): 557-570.

Bergfeld, B., van Herwijnen, A., Bobillier, G., Rosendahl, P.L., Weißgraeber, P., Adam, V., Dual, J. and Schweizer, J., 2023. Temporal evolution of crack propagation characteristics in a weak snowpack layer: conditions of crack arrest and sustained propagation. Nat. Hazards Earth Syst. Sci., 23(1): 293-315.

Bergfeld, B., van Herwijnen, A., Reuter, B., Bobillier, G., Dual, J. and Schweizer, J., 2021. Dynamic crack propagation in weak snowpack layers: insights from high-resolution, high-speed photography. Cryosphere, 15(7): 3539-3553.

Bobillier, G., Bergfeld, B., Dual, J., Gaume, J., van Herwijnen, A. and Schweizer, J., 2021. Micro-mechanical insights into the dynamics of crack propagation in snow fracture experiments. Sci. Rep., 11: 11711.

Fierz, C., Armstrong, R.L., Durand , Y., Etchevers, P., Greene, E., McClung, D.M., Nishimura, K., Satyawali, P.K. and Sokratov, S.A., 2009. The International Classification for Seasonal Snow on the Ground. HP-VII Technical Documents in Hydrology, 83. UNESCO-IHP, Paris, France, 90 pp.

Fond, C. and Schirrer, R., 2001. Influence of crack speed on fracture energy in amorphous and rubber toughened amorphous polymers. Plast. Rubber Compos., 30(3): 116-124.

Freund, L.B., 1990. Dynamic Fracture Mechanics. Cambridge Monographs on Mechanics. Cambridge University Press, Cambridge, 563 pp.

Gaume, J., Gast, T., Teran, J., van Herwijnen, A. and Jiang, C., 2018. Dynamic anticrack propagation in snow. Nat. Commun., 9(1): 3047.

McClung, D.M., 1981. Fracture mechanical models of dry slab avalanche release. J. Geophys. Res., 86(B11): 10783-10790.

Rosendahl, P.L. and Weissgraeber, P., 2020. Modeling snow slab avalanches caused by weak-layer failure - Part 1: Slabs on compliant and collapsible weak layers. Cryosphere, 14(1): 115-130.

Schweizer, J., Jamieson, J.B. and Schneebeli, M., 2003. Snow avalanche formation. Rev. Geophys., 41(4): 1016.

Trottet, B., Simenhois, R., Bobillier, G., Bergfeld, B., van Herwijnen, A., Jiang, C.F.F. and Gaume, J., 2022. Transition from sub-Rayleigh anticrack to supershear crack propagation in snow avalanches. Nat. Phys., 18(9): 1094–1098.

van Herwijnen, A. and Jamieson, B., 2005. High-speed photography of fractures in weak snowpack layers. Cold Reg. Sci. Technol., 43(1-2): 71-82.